Thermally Stable Pt-Mesoporous Silica Core-Shell Nanocatalysts for High Temperature Reactions

Sang Hoon Joo, Jeong Young Park, Chia-Kuang Tsung, Yusuke Yamada, Peidong Yang and Gabor A. Somorjai*

Department of Chemistry, University of California, Berkeley, and Chemical Sciences and Materials Sciences Divisions, Lawrence Berkeley National Laboratory, Berkeley, California 94720, USA.

** e-mail: somorjai@berkeley.edu*

Recent advances in colloidal synthesis enabled the precise control of size, shape and composition of catalytic metal nanoparticles, allowing their use as model catalysts for systematic investigations of the atomic-scale properties affecting catalytic activity and selectivity. The organic capping agents stabilizing colloidal nanoparticles, however, often limit their application in high-temperature catalytic reactions. Here we report the design of a high-temperature stable model catalytic system that consists of Pt metal core coated with a mesoporous silica shell (Pt@mSiO_2). While inorganic silica shells encaged the Pt cores up to 750 ^oC in air, the mesopores directly accessible to Pt cores made the Pt@mSiO_2 nanoparticles as catalytically active as bare Pt metal for ethylene hydrogenation and CO oxidation. The high thermal stability of Pt@mSiO_2 nanoparticles permitted high-temperature CO oxidation studies, including ignition behavior, which was not possible for bare

Pt nanoparticles because of their deformation or aggregation. The results suggest that the Pt@mSiO$_2$ nanoparticles are excellent nanocatalytic systems for high-temperature catalytic reactions or surface chemical processes, and the design concept employed in the Pt@mSiO$_2$ core-shell catalyst can be extended to other metal-metal oxide compositions.

To design high performance catalysts in terms of activity, selectivity and resistance to deactivation, understanding the properties affecting catalytic performance are of great importance[1-4]. Over the past few decades, model catalytic systems, including metal single crystals and lithographically fabricated metal nanostructures, have successfully been used to uncover atomic-scale characteristics, such as surface structures and particle size, that are critical to catalytic activity and selectivity[5-8]. Recent advances in colloid chemistry allowed catalytic nanoparticles to be readily prepared with tunable particle size, shape and composition[9-13]. Starting with colloidal nanoparticles, 2-dimensonal (2D) and 3-dimensional (3D) model catalysts have been developed which are composed of arrays of nanoparticles on a flat substrate and nanoparticles dispersed on high-surface-area mesoporous oxide support, respectively. These model catalytic systems have enabled systematic investigations of the effects of particle size[14], shape[15-17] and composition[18,19] on catalytic properties.

Catalytic studies of colloidal nanoparticles have shown that the thermal and chemical stabilities of nanoparticle catalysts are crucial. Colloidal nanoparticles are usually prepared in the presence of organic capping agents, such as polymers or surfactants, that prevent the aggregation of nanoparticles in solution. At high temperatures, typically above 300 ^{o}C, however, the organic capping layers can

decompose and the metal nanoparticles can deform and aggregate. As a result, the size, shape and composition of nanoparticles during or after high temperature reactions could be different from those of pristine nanoparticles. Many industrially important catalytic processes, including CO oxidation[20-25], partial oxidation[26] and cracking[27] of hydrocarbons, and combustion[28] reactions, are performed at temperatures above 300 ^{o}C. In this regard, model catalysts that are stable at high reaction temperatures are high in demand.

In this work, we designed core-shell particle configurations and prepared the nanoparticles with high thermal stability. The core-shell structures have important implications in catalysis[29]. The outer shells isolate the catalytically active nanoparticle cores and prevent the possibility of sintering of core particles during catalytic reactions at high temperatures. Additionly, the synergistic effects of metal-support interfaces may be maximized where such interfaces are important in catalytic performances.

Herein, we report the preparation of Pt-mesoporous silica core-shell (Pt@mSiO_2) nanoparticles that are thermally stable at high temperatures. We performed CO oxidation and ethylene hydrogenation reactions to explore the catalytic activities of the Pt@mSiO_2 core-shell nanoparticles. The core-shell structured Pt@mSiO_2 nanoparticles were prepared in three steps (Figure 1): (i) synthesis of Pt nanoparticles using tetradecyltrimethylammonum bromide (TTAB) as the capping agent, (ii) silica polymerization around the Pt cores generating the as-synthesized Pt@SiO_2 mesostructures and (iii) removal of the TTAB molecules by calcination to produce the Pt@mSiO_2 core-shell nanoparticles. The Pt@mSiO_2 consisted of 14 nm Pt cores and 17 nm thick mesoporous silica shells. The reacting molecules are directly accessible to the Pt cores through the mesopores within the silica shells and the product molecules can

readily exit through these mesopores. The Pt cores were encaged within the silica shells at temperatures up to 750 °C in air. The Pt@mSiO_2 nanoparticle catalysts exhibited catalytic activity similar to TTAB-capped Pt nanoparticles for ethylene hydrogenation and CO oxidation. Significantly, the high thermal stability of Pt@mSiO_2 nanoparticles enabled the study of ignition behavior during the Pt nanoparticle catalyzed CO oxidation process. The high thermal stability, as well as uniform mesoporous shell structure, suggested that the Pt@mSiO_2 core-shell nanoparticles are an excellent nanoparticle system for catalytic reactions or surface chemical processes that occur at high temperatures.

The TEM images for TTAB-capped Pt and as-synthesized Pt@SiO_2 nanoparticles are displayed in Figure 2. The TTAB-capped Pt nanoparticles displayed in Figure 2a were composed of a mixture of cubes (70 %), cuboctahedra (26 %) and irregular shapes (4 %) and exhibited an average particle size around 14.3 nm in diagonal distance. The surfaces of these Pt cubes are stabilized by the bilayer of the TTAB surfactants[30]. These surface capping TTAB surfactants were also used as structure directing templates for the polymerization of silicates by a sol-gel process, as demonstrated in the synthesis of MCM-41-like ordered mesoporous silicas[31,32]. The silica-TTAB layer was formed around the Pt nanoparticles under basic conditions (pH = 10 – 11) through an electrostatic interaction between the cationic (TTAB) and anionic (silicate) species. The TEM images of as-synthesized Pt@SiO_2 obtained under optimized experimental conditions (Pt colloid : TEOS = 1 : 4.5), where each Pt particle is encapsulated by a silica layer, are shown in Figure 1b and c. The average thickness of the silica layer surrounding the Pt core was around 17 nm. Figure 2c displays the closely

assembled structure of the Pt@SiO_2 nanoparticles in a large area, which was formed by drop casting on a TEM grid. The XRD patterns for Pt and Pt@SiO_2 nanoparticles (Figure 2d) revealed that the crystal structure (face centered cubic) TTAB-capped Pt nanoparticles was maintained after the formation of the silica layer on Pt.

Most (~ 95%) of the as-synthesized Pt@SiO_2 nanoparticles shown in Figure 2b and 2c exhibited the core-shell structures, where each Pt particle is encaged within a silica shell. The configuration of core-shell nanoparticles was tuned by changing the concentration of the silica source (TEOS) added for the silica polymerization. If the concentration of TEOS was decreased compared to the amount required for optimized condition, the silica shell contained multiple Pt particles (Figure S1a). Increasing the amount of TEOS resulted in the formation of a mixture of Pt@mSiO_2 and amorphous silica particles without Pt cores (Figure S1b). This synthetic strategy can be generally applicable to nanoparticles with differing composition, size and shape. For instance, smaller size 8.5 nm TTAB-capped Pt nanoparticles can be readily converted into Pt@SiO_2 core-shell particles, as shown in Figure S2.

The as-synthesized Pt@SiO_2 nanoparticles contained a significant amount of the TTAB surfactants that are unfavorable for reactant and product molecular diffusion in catalytic applications. To remove the TTAB surfactants, the as-synthesized Pt@SiO_2 sample was calcined at 350 °C for 2 h in static air to yield mesoporous Pt@mSiO_2 nanoparticles. The TEM images of Pt@mSiO_2 nanoparticles after calcination (Figure 3a and 3b) exhibited mesopores of 2 – 3 nm in the silica shells. The porosity of Pt@mSiO_2 was confirmed by nitrogen physisorption. The nitrogen adsorption-desorption isotherms of Pt@mSiO_2 calcined at 350 °C (Figure 4a) revealed that these nanoparticles are

mesoporous, as identified by the increase of the adsorption amount in the relative pressure (P/P_0) range of 0.2 to 0.3. The pore size distribution curve calculated from adsorption branch of isotherms (Figure 4b) exhibited a maximum at 2.3 nm and the BET surface area of Pt@mSiO_2 was calculated to be 440 m^2 g^{-1}, indicating the highly mesoporous nature of the silica shell.

For core-shell nanoparticles to be catalytically active, direct access of reactive molecules to the core particles is of significant importance. In previous examples of metal-mesoporous silica core-shell particles[33-35], an intermediate protecting amorphous silica layer was often sandwiched between the metal core and the mesoporous silica layer, thus hampering direct access of reactants to the metal core. In our design of these core-shell particles, the mesoporous silica layer was directly formed on the Pt cores. The accessibility of gas molecules was directly proven by chemisorption measurements. Hydrogen chemisorption over the Pt@mSiO_2 catalyst gave a dispersion value of 8 ± 0.5 %, which is comparable with the ratio of surface atoms (11 %) on the Pt particle, as calculated by geometric considerations[36].

After calcination at 350 °C, the spherical core-shell shape of the as-synthesized Pt@SiO_2 particles was maintained, as can be seen by comparing the TEM images before (Figure 2b) and after (Figure 3a) calcination. The shape of the Pt cores inside Pt@mSiO_2 became slightly rounder after calcination, which is presumably due to the melting of the Pt particles at the Pt-silica interface, as reported earlier[37]. However, a closer observation of the Pt core by high resolution TEM image in Figure S3 revealed that the Pt core continued to be facetted and single crystalline after thermal treatment under air. The stability of Pt@mSiO_2 core-shell nanoparticles at higher temperatures was investigated

by heating the sample to 550 °C and 750 °C in air. After the calcination at 550 °C (Figure 3c), the core-shell morphology of Pt@mSiO_2 nanoparticles was preserved. Even upon heating the sample as high as 750 °C, the morphology of most Pt@mSiO_2 nanoparticles was maintained and the Pt cores were still encaged within the silica shells (Figure 3d), indicating high thermal stability of Pt@mSiO_2 core-shell nanoparticles. It is interesting to note that in the case of sample calcined at 750 °C, some of core-shell particles possessing larger Pt cores and Pt-free hollow silica particles were found. It seemed that Pt cores in Pt@mSiO_2 nanoparticles diffused around 750 °C through the mesoporous silica shell into the neighboring Pt@mSiO_2 particles. A detailed study of the thermal evolution of Pt@mSiO_2 nanoparticles is currently being investigated.

The noble metal-metal oxide core-shell structured nanoparticles have recently been exploited for catalytic applicatons[38-43]. Examples include Pt-CoO yolk-shell nanoparticles[38], PVP capped Pt encapsulated in mesoporous silica[39], Pt nanoparticles entrapped in hollow carbon shells[40], and Au nanoparticles within hollow zirconia[41] and hollow silica[42] and tin oxide shells[43]. Our present design of Pt@mSiO_2 core-shell nanoparticles allows the direct access of reactive molecules to the catalytically active core metals. In addition, the Pt cores within the silica layer can be encaged even after high-temperature treatments while the faceted nature of the particle is preserved, showing great promise for use in high-temperature catalytic reactions.

The catalytic activity of Pt@mSiO_2 nanoparticles was investigated in ethylene hydrogenation. The ethylene hydrogenation was performed at 10 Torr of ethylene, 100 Torr of H_2, with the balance He (see Supplementary Information for experimental details). The Pt@mSiO_2 exhibited a TOF of 6.9 s^{-1} at 25 °C and activation energy of 8.1 kcal mol^{-}

[1]. The TOF and activation energy are similar to those of the Pt single crystal, colloidal Pt nanoparticle loaded SBA-15 model catalysts, and other supported catalysts (see Table S1). It is worth noting that the Pt@mSiO_2 nanoparticles exhibited an order of magnitude higher TOF than the Pt@CoO yolk-shell nanoparticles[38]. The higher activity of Pt@mSiO_2 is likely due to the more facile diffusion and transport of the reactants and products through the mesoporous silica shells in Pt@mSiO_2 than the CoO shell in Pt@CoO where the grain boundaries in CoO were proposed as entry points for the molecules[38].

The high-temperature catalytic properties of Pt@mSiO_2 core-shell nanoparticles were explored by using CO oxidation as a model reaction. The catalytic oxidation of CO to CO_2 over platinum group metals has been one of the most widely studied surface reactions due to its significance for emission control and fuel cells[20-25]. In particular, from the mechanistic point of view, the CO oxidation reaction is intriguing as the reaction proceeds via different mechanisms below and above the ignition temperature. For the CO oxidation reaction, the Pt@mSiO_2 and Pt nanoparticles were deposited on a silicon wafer using the Langmuir-Blodgett (LB) technique. CO oxidation was performed with excess O_2 (40 Torr CO, 100 Torr O_2, with the balance He) in the temperature range of 240 to 340 °C. Figure 5 presents the activity of the Pt@mSiO_2. Two distinct reaction regimes are observed as a function of temperature, which indicated an ignition temperature around 290 – 300 °C. For comparison, the TTAB-capped Pt nanoparticle catalyst on the silicon wafer was also tested for CO oxidation. The activity of the Pt@mSiO_2 catalyst was as high as TTAB-capped Pt nanoparticles, indicating that the silica shells in the Pt@mSiO_2 nanoparticles were porous enough to provide access to the Pt cores, which is consistent

with our chemisorption and TEM studies. Figure 6 comparatively displays SEM and TEM images of TTAB-capped Pt nanoparticle arrays on the silicon wafer and Pt dispersed inside the mesopores of MCF mesoporous silica (Pt/MCF), as well as the core-shell Pt@mSiO_2 before and after CO oxidation at 300 °C. The Pt@mSiO_2 catalyst after CO oxidation at 330 ^{o}C maintained the morphology of calcined particles (Figure 6b). More importantly, the faceted and crystalline nature of the Pt cores in the Pt@mSiO_2 catalyst was preserved after the reaction, as shown in Figure S4. However, the TTAB-capped Pt on silicon wafer (Figure 6d) and Pt/MCF (Figure 6f) exhibited severe aggregation of Pt particles after CO oxidation at 300 ^{o}C, which hampered the quantitative study of CO oxidation above the ignition temperature regime. The XPS spectra of O1s peaks of Pt@mSiO_2 revealed that the Pt core was partially oxidized after CO oxidation (Figure S5 in Supplementary Information).

The ignition temperature during CO oxidation over the Pt@mSiO_2 catalyst is 290 – 300 °C, which lies between that of Pt (100) (227 °C) and Pt (111) (347 °C) single crystals[25]. The Pt cores encaged in Pt@mSiO_2 nanoparticles are mostly composed of cubic and cuboctahedron shapes, exposing mostly (100) and (111) surfaces, which explains the reason for the ignition temperature of the Pt@mSiO_2 nanoparticles to be between those of Pt (100) and Pt (111) single crystals. The Pt@mSiO_2 nanoparticles exhibited lower activation energies (27.5 and 9.8 kcal mol^{-1} for below and above ignition temperature, respectively) than Pt (111) single crystal (42 and 14 kcal mol^{-1})[24] and (100) single crystal (32.9 kcal mol^{-1} for below ignition)[22]. For catalytic reactions on the surface to occur, the reacting molecules, reaction intermediates and products must alter their bond distances to allow rapid rearrangement. A relatively small number of bonds must

also be broken and reformed as the catalytic chemistry occurs. The chemical bonds rearrange more easily on nanoparticles, where fewer atoms participate in the restructuring during catalytic turnover than on single crystal surfaces and this phenomena might be responsible for the origin of lower activation energies.

In summary, the core-shell structured Pt-mesoporous silica (Pt@mSiO_2) nanoparticles were designed as high-temperature model catalysts. The Pt@mSiO_2 nanoparticles maintained their core-shell configurations up to 750 °C and exhibited high catalytic activity for ethylene hydrogenation and CO oxidation. The mesoporous silica coating chemistry on nanoparticle surface is straightforward. Thus, the method can potentially be extended to other nanoparticle cores with different composition, size, and shape and to other shell compositions. The CO oxidation study highlights the role of the thermally stable inorganic silica shell in the Pt@mSiO_2 nanoparticles that permit the study of catalytic reactions or surface phenomena taking place at high temperatures. Further application of core-shell catalysts to high-temperature reactions, such as partial oxidation and cracking of hydrocarbon and catalytic combustion, appears possible.

Methods

Synthesis of TTAB-capped Pt and Pt@mSiO_2 core-shell nanoparticles. The synthesis of TTAB-capped Pt nanoparticles was performed by following the reported method with a modification[30]. The detailed synthesis procedure for Pt nanoparticles has been described in the Supplementary Information. The Pt@mSiO_2 core-shell nanoparticles were prepared by polymerizing the silica layer around the surface of Pt nanoparticles via a sol-gel process[33-35,44-46]. The Pt nanoparticle colloid (4.5×10^{-5} mole) dispersed in 5 mL of DI

water was added to 35.5 mL of DI water. A NaOH solution (1.0 mL of 0.05 M) was added to the aqueous Pt colloid solution with stirring to adjust the pH of the solution to around 10 - 11. To this basic solution, a controlled amount of 10 vol% tetraethylorthosilicate (TEOS) diluted with methanol was added to initiate the silica polymerization. The as-synthesized Pt@SiO_2 was calcined at 350 °C or higher for 2 h in static air to remove TTAB surfactants to generate Pt@mSiO_2 particles. The 2D model catalyst systems were fabricated by depositing the colloidal Pt and Pt@SiO_2 nanoparticles on a silicon wafer using the LB technique (see Supplementary Information). MCF mesoporous silica with large mesopores, around 30 nm, was synthesized following the method found in the literature[47] and TTAB-capped Pt nanoparticle was incorporated inside the pores of the MCF silica by capillary inclusion[48] to produce the 3D model catalyst.

Characterization. The particle size and shape were analyzed with transmission electron microscope (TEM) images using a Philips/FEI Tecnai 12 microscope operating at 100 kV and an FEI Tecnai G^2 S-Twin electron microscope operating at 200 kV. X-ray diffraction (XRD) patterns were measured on a Bruker D8 GADDS diffractometer using Co K_α radiation (1.79 Å). Nitrogen physisorption experiments were performed using a Quantachrome Autosorb-1 analyzer at – 196 °C. Before the measurement, degassing was conducted at 200 °C for 12 h to remove possible moisture. Hydrogen chemisorption was also carried out with a Quantachrome Autosorb-1 at 30 ^oC. Before the chemisorptions, the sample was heated to 300 ^oC for 1 h under H_2 and evacuated at 310 ^oC for 1.5 h, then cooled down to room temperature. The morphology and chemical composition of the 2-D LB films were characterized with a scanning electron microscope (SEM) and X-ray

photoelectron spectroscopy (XPS), respectively. SEM images were taken on a Zeiss Gemini Ultra-55 with a beam energy of 5 kV. XPS spectra were taken on a 15 kV, 350 Watt PHI 5400 ESCA/XPS system equipped with an Al anode X-ray source.

CO oxidation measurements. CO oxidation studies were performed in an ultrahigh vacuum chamber with a base pressure of 5.0×10^{-8} Torr[19]. The reactions were carried out under excess O_2 conditions: 40 Torr CO, 100 Torr O_2, and 620 Torr He. The gases were circulated through the reaction line by a Metal Bellows recirculation pump at a rate of 2 L min^{-1}. The volume of the reaction loop is 1.0 L. An HP Series II gas chromatograph equipped with a thermal conductivity detector and a 15′, 1/8″ SS 60/80 Carboxen-1000 (Supelco) was used to separate the products for analysis. The measured reaction rates are reported as turnover frequencies (TOF) and are measured in units of product molecules of CO_2 produced per metal surface site per second of reaction time. The number of metal sites is calculated by geometrical considerations based on SEM measurements of the surface area of a nanoparticle array.

References

1. Bell, A. T. The impact of nanoscience on heterogeneous catalysis. *Science* **299**, 1688–1691 (2003).
2. Schlögl, R. & Abd Hamid, S. B. Nanocatalysis: mature science revisited or something really new? *Angew. Chem. Int. Ed.* **43**, 1628–1637 (2004).
3. Somorjai, G. A., Contreras, A. M., Montano, M. & Rioux, R. M. Clusters, surfaces, and catalysis. *Proc. Natl. Acad. Sci. USA* **103**, 10577–10583 (2006).
4. Thomas, J. M. Heterogeneous catalysis: enigmas, illusions, challenges, realities,

and emergent strategies of design. *J. Chem. Phys.* **128**, 182502 (2008)

5. Somorjai, G. A. *Introduction to Surface Chemistry and Catalysis* (Wiley, New York, 1994).

6. Over, H. *et al*. Atomic-scale structure and catalytic reactivity of the RuO_2(110) surface. *Science* **287**, 1474–1476 (2000).

7. Greeley, J. & Mavrikakis, M. Alloy catalysts designed from first principles. *Nat. Mater*. **3**, 810–815 (2004).

8. Stamenkovic, V. R. *et al*. Improved oxygen reduction activity on Pt_3Ni(111) via increased surface site availability. *Science* **315**, 493-497 (2007).

9. Roucoux, A., Schulz, J. & Patin, H. Reduced transition metal colloids: a novel family of reusable catalysts? *Chem. Rev.* **102**, 3757–3778 (2002).

10. Park, J., Joo, J., Kwon, S. G., Jang, Y. & Hyeon, T. Synthesis of monodisperse spherical nanocrystals. *Angew. Chem. Int. Ed.* **46**, 4630–4660 (2007).

11. Tao, A. R., Habas, S. & Yang, P. Shape control of colloidal metal nanocrystals. *Small* **4**, 310–325 (2008).

12. Ahmadi, T. S., Wang, Z. L., Green, T. C., Henglein, A. & El-Sayed, M. A. Shape-controlled synthesis of colloidal platinum nanoparticles. *Science* **272**, 1924–1926 (1996).

13. Sun, Y. & Xia, Y. Shape-controlled synthesis of gold and silver nanoparticles. *Science* **298**, 2176–2179 (2002).

14. Song, H. *et al*. Hydrothermal growth of mesoporous SBA-15 silica in the presence of PVP-stabilized Pt nanoparticles: synthesis, characterization, and catalytic properties. *J. Am. Chem. Soc.* **128**, 3027–3037 (2006).

15. Narayanan, R. & El-Sayed, M. A. Shape-dependent catalytic activity of platinum nanoparticles in colloidal solution. *Nano Lett.* **4**, 1343–1348 (2004).

16. Tian, N., Zou, Z.-Y., Sun, S.-G., Ding, Y. & Wang, Z. L. Synthesis of tetrahexahedral platinum nanocrystals with high-index facets and high electro-oxidation activity. *Science* **316**, 732–735 (2007).

17. Bratlie, K. M., Lee, H., Komvopoulos, K., Yang, P. & Somorjai, G. A. Platinum nanoparticle shape effects on benzene hydrogenation selectivity. *Nano Lett.* **7**, 3097–3101 (2007).

18. Alayoglu, S., Nilekar, A. U., Mavrikakis, M. & Eichhorn, B. Ru–Pt core–shell nanoparticles for preferential oxidation of carbon monoxide in hydrogen. *Nat. Mater.* **7**, 333–338 (2008).

19. Park, J. Y., Zhang, Y., Grass, M., Zhang, T. & Somorjai, G. A. Tuning of catalytic CO oxidation by changing composition of Rh–Pt bimetallic nanoparticles. *Nano Lett.* **8**, 673–677 (2008).

20. Langmuir, I. The mechanism of the catalytic action of platinum in the reactions $2CO + O_2 = 2CO_2$ and $2H_2 + O_2 = 2H_2O$. *Trans. Frad. Soc.* 621–654 (1922).

21. Campbell, C. T., Ertl, G., Kuipers, H. & Segner, J. A molecular beam study of the catalytic oxidation of CO on a Pt(111) surface. *J. Chem. Phys.* **73**, 5862-5873 (1980).

22. Berlowitz, P. J., Peden, C. H. F. & Goodman, D.W. Kinetics of CO oxidation on single-crystal Pd, Pt, and Ir. *J. Phys. Chem.* **92**, 5213–5221 (1988).

23. Chen, M. S. et al. Highly active surfaces for CO oxidation on Rh, Pd, and Pt. *Surf. Sci*. **601**, 5326–5331 (2007).

24. Su, X. C., Cremer, P. S., Shen, Y. R. & Somorjai, G. A. High-pressure CO oxidation on Pt(111) monitored with infrared-visible sum frequency generation (SFG). *J. Am. Chem. Soc.* **119**, 3994–4000 (1997).

25. McCrea, K. R., Parker, J. S. & Somorjai, G. A. The role of carbon deposition from CO dissociation on platinum crystal surfaces during catalytic CO oxidation: effects on turnover rate, ignition temperature, and vibrational spectra. *J. Phys. Chem.* **106**, 10854–10863 (2002).

26. Zaera, F. The surface chemistry of hydrocarbon partial oxidation catalysis. *Catal. Today* **81**,149–157 (2003).

27. Huber, G. W. & Corma, A. Synergies between bio- and oil refineries for the production of fuels from biomass. *Angew. Chem. Int. Ed.* **46**, 7184–7201 (2007).

28. Ciuparu, D., Lyubovsky, M. R., Altman, E., Pfefferle, L. D. & Datye, A. Catalytic combustion of methane over palladium-based catalysts. *Catal. Rev.* **44**, 593–649 (2002)

29. Somorjai, G. A. & Rioux, R. M. High technology catalysts towards 100% selectivity. Fabrication, characterization and reaction studies. *Catal. Today* **100**, 201–215 (2005).

30. Lee, H. *et al*. Morphological control of catalytically active platinum nanocrystals. *Angew. Chem. Int. Ed.* **45**, 7824–7828 (2006).

31. Kresge, C. T., Leonowicz, M. E., Roth, W. J., Vartuli, J. C. & Beck, J. S. Ordered mesoporous molecular sieves synthesized by a liquid-crystal mechanism. *Nature* **359**, 710–712 (1992).

32. Corma, A. From microporous to mesoporous molecular sieve materials and their

use in catalysis. *Chem. Rev.* **97**, 2373–2419 (1997).

33. Kim, M., Sohn, K., Na, H. B. & Hyeon, T. Synthesis of nanorattles composed of gold nanoparticles encapsulated in mesoporous carbon and polymer shells. *Nano Lett.* **2**, 1383–1387 (2002).

34. Nooney, R. I., Thirunavukkarasu, D., Chen, Y., Josephs, R. & Ostafin, A. E. Self-assembly of mesoporous nanoscale silica/gold composites *Langmuir* **19**, 7628–7637 (2003).

35. Botella, P., Corma, A. & Navarro, M. T. Single gold nanoparticles encapsulated in monodispersed regular spheres of mesostructured silica produced by pseudomorphic transformation. *Chem. Mater.* **19**, 1979–1983 (2007).

36. van Hardeveld, R. & Hartog, F. The statistics of surface atoms and surface sites on metal crystals. *Surf. Sci.* **15**, 189–230 (1969).

37. Yu, R., Song, H., Zhang, X.-F. & Yang, P. Thermal wetting of platinum nanocrystals on silica surface. *J. Phys. Chem. B* **109**, 6940–6943 (2005).

38. Yin, Y. *et al*. Formation of hollow nanocrystals through the formation of nanoscale Kirkendall effect. *Science* **304**, 711–714 (2004).

39. Lin, K.-J., Chen, L.-J., Prasad, M. R. & Cheng, C. Y. Core-shell synthesis of a novel, spherical, mesoporous silica/platinum nanocomposite: Pt/PVP@MCM-41. *Adv. Mater*. **16**, 1845–1849 (2004).

40. Ikeda, S. *et al*. Ligand-free platinum nanoparticles encapsulated in a hollow porous carbon shell as a highly active heterogeneous hydrogenation catalyst. *Angew. Chem. Int. Ed.* **45**, 7063–7066 (2006).

41. Arnal, P. M., Comotti, M. & Schüth, F. High-temperature-stable catalysts by

hollow sphere encapsulation. *Angew. Chem. Int. Ed.* **45**, 8224–8227 (2006).

42. Lee, J., Park, J. C. & Song, H. A nanoreactor framework of a Au@SiO_2 yolk/shell structure for catalytic reduction of *p*-nitrophenol. *Adv. Mater*. **20**, 1523–1528 (2008).

43. Yu, K., Wu, Z., Zhao, Q., Li, B. & Xie, Y. High-temperature-stable Au@SnO_2 core/shell supported catalyst for CO oxidation. *J. Phys. Chem. C* **112**, 2244–2247 (2008)

44. Liz-Marzan, L. M., Giersig, M. & Mulvaney, P. Synthesis of nanosized gold-silica core-shell particles. *Langmuir* **12**, 4329–4335 (1996).

45. Lu, Y., Yin, Y., Li, Z.-Y. & Xia, Y. Synthesis and self-assembly of Au@SiO_2 core-shell colloids. *Nano Lett.* **2**, 785–788 (2002).

46. Gorelikov, I. & Matsuura, N. Single-step coating of mesoporous silica on cetyltrimethyl ammonium bromide-capped nanoparticles. *Nano Lett.* **8**, 369–373 (2008).

47. Schmidt-Winkel, P. *et al*. Microemulsion templating of siliceous mesostructured cellular foams with well-defined ultralarge mesopores. *Chem. Mater*. **12**, 686–696 (2000).

48. Rioux, R. M., Song, H., Hoefelmeyer, J. D., Yang, P. & Somorjai, G. A. High-surface-area catalyst design: synthesis, characterization, and reaction studies of platinum nanoparticles in mesoporous SBA-15 silica. *J. Phys. Chem. B* **109**, 2192–2202 (2005).

Supplementary Information accompanies this paper on www.nature.com/naturematerials.

Acknowledgements

This work was supported by the Director, Office of Science, Office of Basic Energy Sciences, Division of Chemical Sciences, Geological and Biosciences of the U.S. Department of Energy under Contract DE-AC03-76SF00098. This work was also supported by the Director, Office of Science, Office of Basic Energy Sciences, Division of Materials Sciences and Engineering of the U.S. Department of Energy under Contract No. DE-AC02-05CH11231. We thank A. Paul Alivisatos and his group for the use of TEM and XRD. We also thank John N. Kuhn, Young-wook Jun and Jungwon Park for helpful comments and Soo Min Ko for illustrations in Figure 1.

Author information

Correspondence and requests for materials should be addressed to G.A.S.

Figure Legends

Figure 1. Schematic representation for the synthesis of Pt-mesoporous silica core-shell (Pt@mSiO$_2$) nanoparticles. Pt nanoparticles were synthesized using TTAB surfactant as the capping agent, and used as the core particles. Secondly, as-synthesized Pt@SiO$_2$ particles were prepared by polymerizing TEOS around the TTAB-capped Pt cores. The as-synthesized Pt@SiO$_2$ particles were subsequently converted to Pt@mSiO$_2$ particles by calcination.

Figure 2. TEM and XRD characterizations of TTAB-capped Pt and as-synthesized Pt@SiO$_2$ core-shell nanoparticles. a-c, TEM images of TTAB-capped Pt (**a**) and as-synthesized Pt@SiO$_2$ nanoparticles (**b,c**). **d**, high angle XRD patterns of Pt and Pt@SiO$_2$ nanoparticles.

Figure 3. Thermal stability of Pt@mSiO$_2$ nanoparticles. TEM images of Pt@mSiO$_2$ nanoparticles after calcination at 350 ℃ (**a,b**), at 550 ℃ (**c**), and at 750 ℃ (**d**).

Figure 4. Structural characterization of Pt@mSiO$_2$ nanoparticles calcined at 350 ℃. a, nitrogen adsorption-desorption isotherms. **b**, pore size distribution calculated from adsorption branch of isotherms.

Figure 5. CO oxidation activity of TTAB-capped Pt (red hollow square) and Pt@mSiO$_2$ (blue solid diamond) nanoparticles.

Figure 6. Change of Pt nanoparticle morphologies before (a-c) and after (d-f) CO oxidation at 300 ℃. SEM images of core-shell Pt@mSiO$_2$ (**a,d**) and TTAB-capped Pt (**b,e**) nanoparticle arrays on 2D silicon wafer, and TEM images of TTAB-capped Pt nanoparticles dispersed on 3D MCF mesoporous silica support (**c,f**).


+ TEOS
NaOH
R.T.
TTAB
removal
TTAB-capped Pt
As-synthesized
Pt@SiO2
Pt@mSiO2

Figure 1

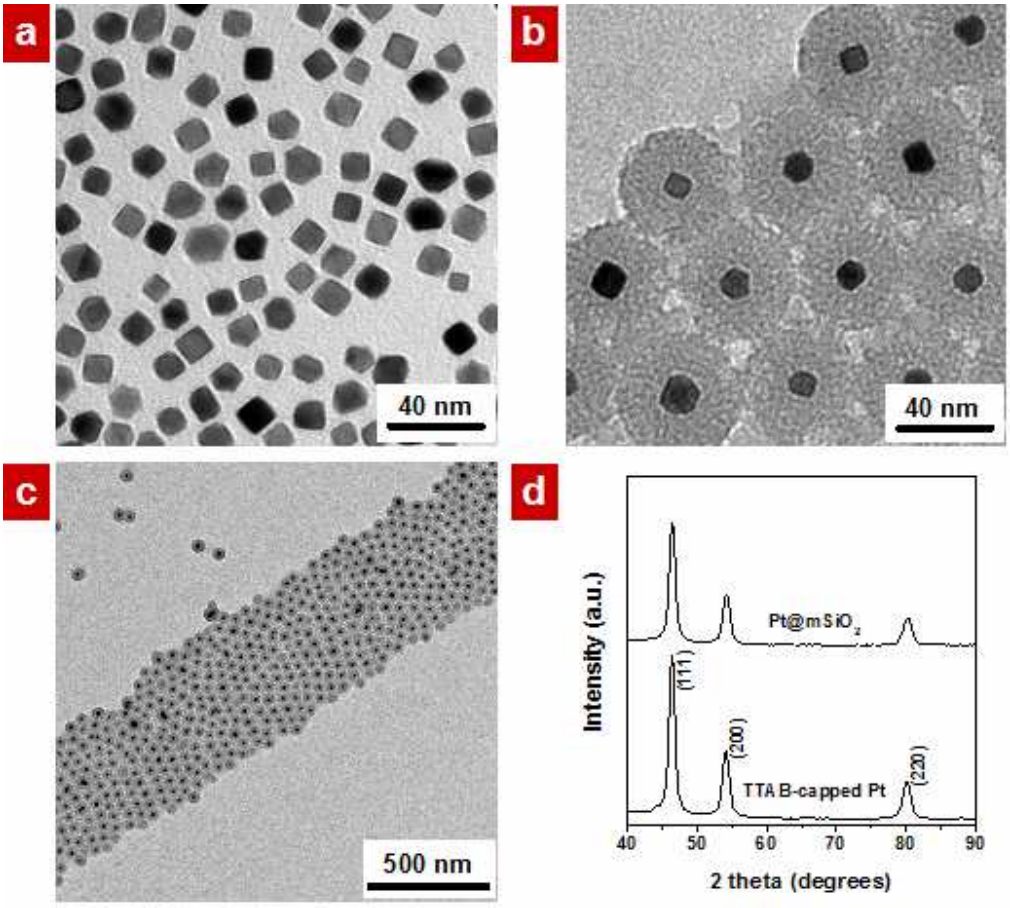
a
40 nm
b
40 nm
c
500 nm
d
Intensity (a.u.)
Pt@mSiO2
(111)
(200)
(220)
TTAB-capped Pt
40
50
60
70
80
90
2 theta (degrees)

Figure 2

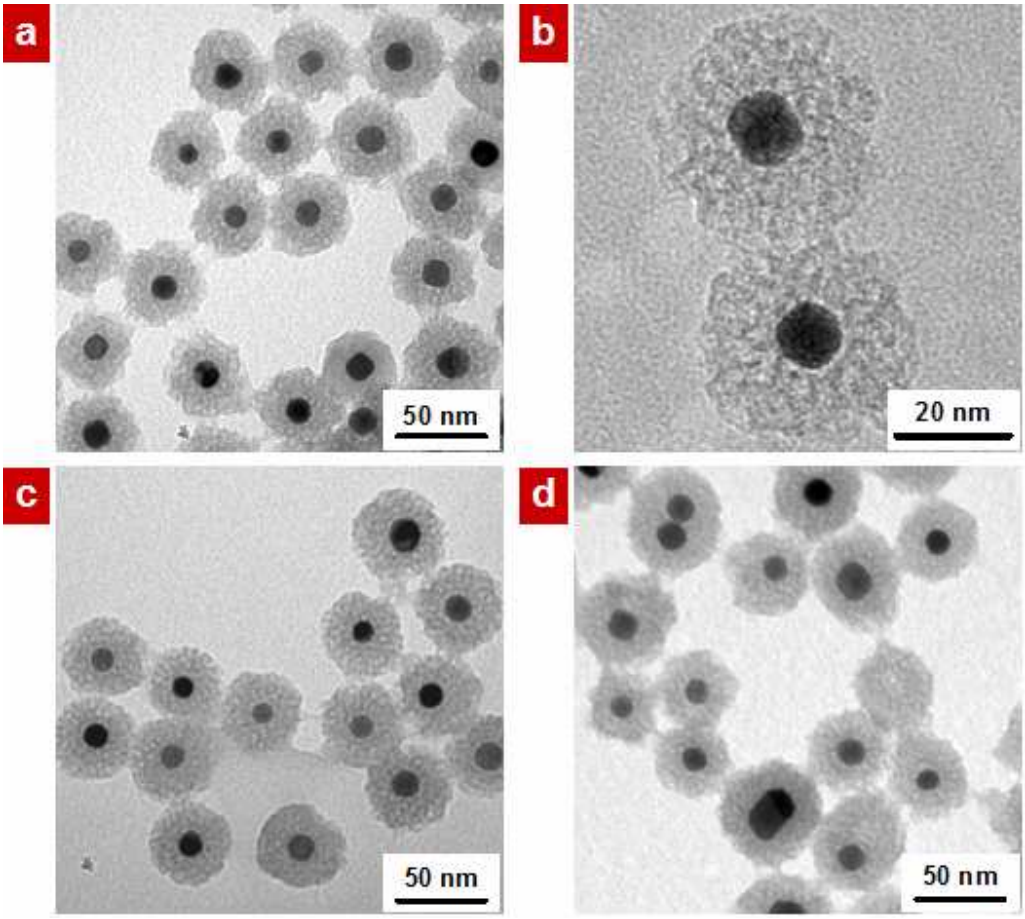

Figure 3

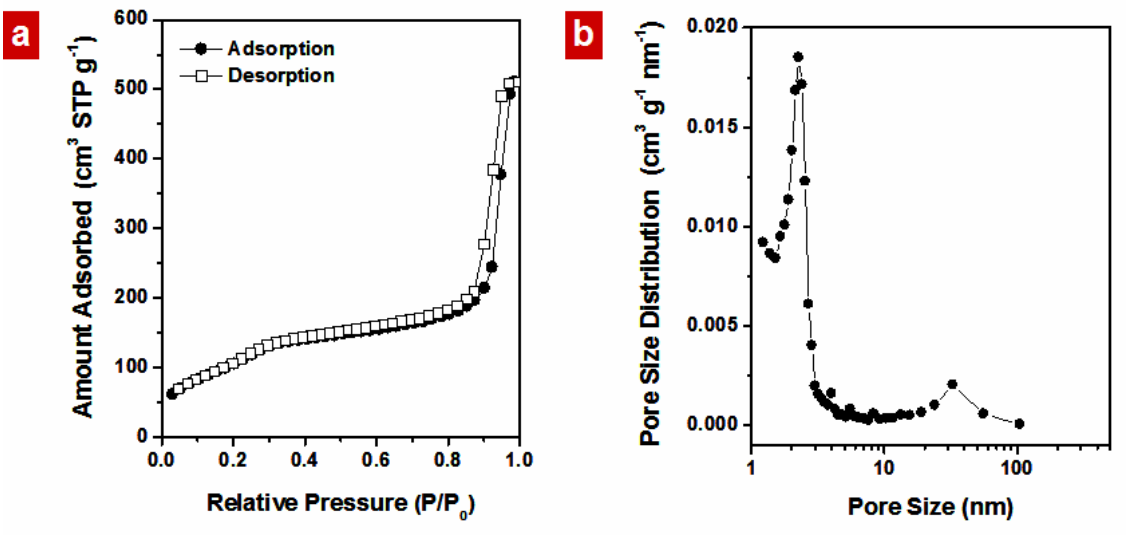
a
Amount Adsorbed (cm^3 STP g^{-1})
Adsorption
Desorption
Relative Pressure (P/P$_0$)
b
Pore Size Distribution (cm^3 g^{-1} nm^{-1})
Pore Size (nm)

Figure 4

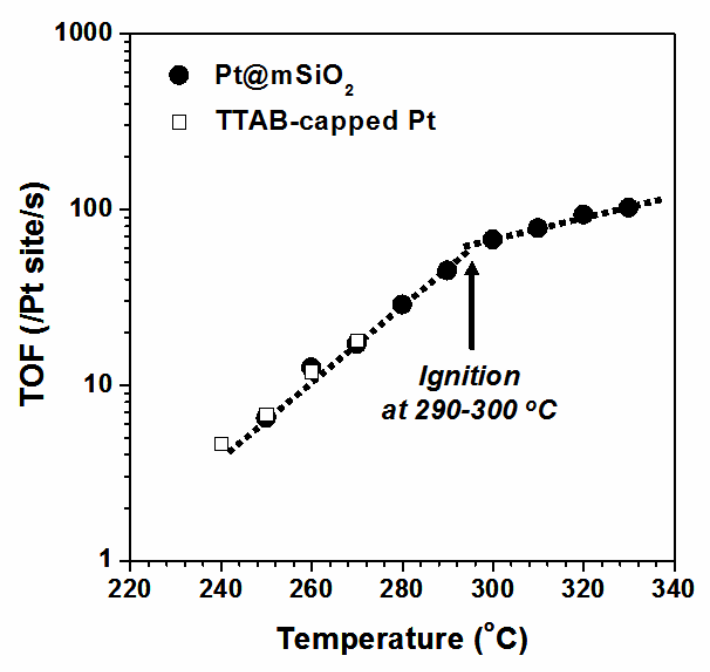
1000
100
10
1
TOF (/Pt site/s)
Pt@mSiO2
TTAB-capped Pt
Ignition
at 290-300 °C
220
240
260
280
300
320
340
Temperature (°C)

Figure 5

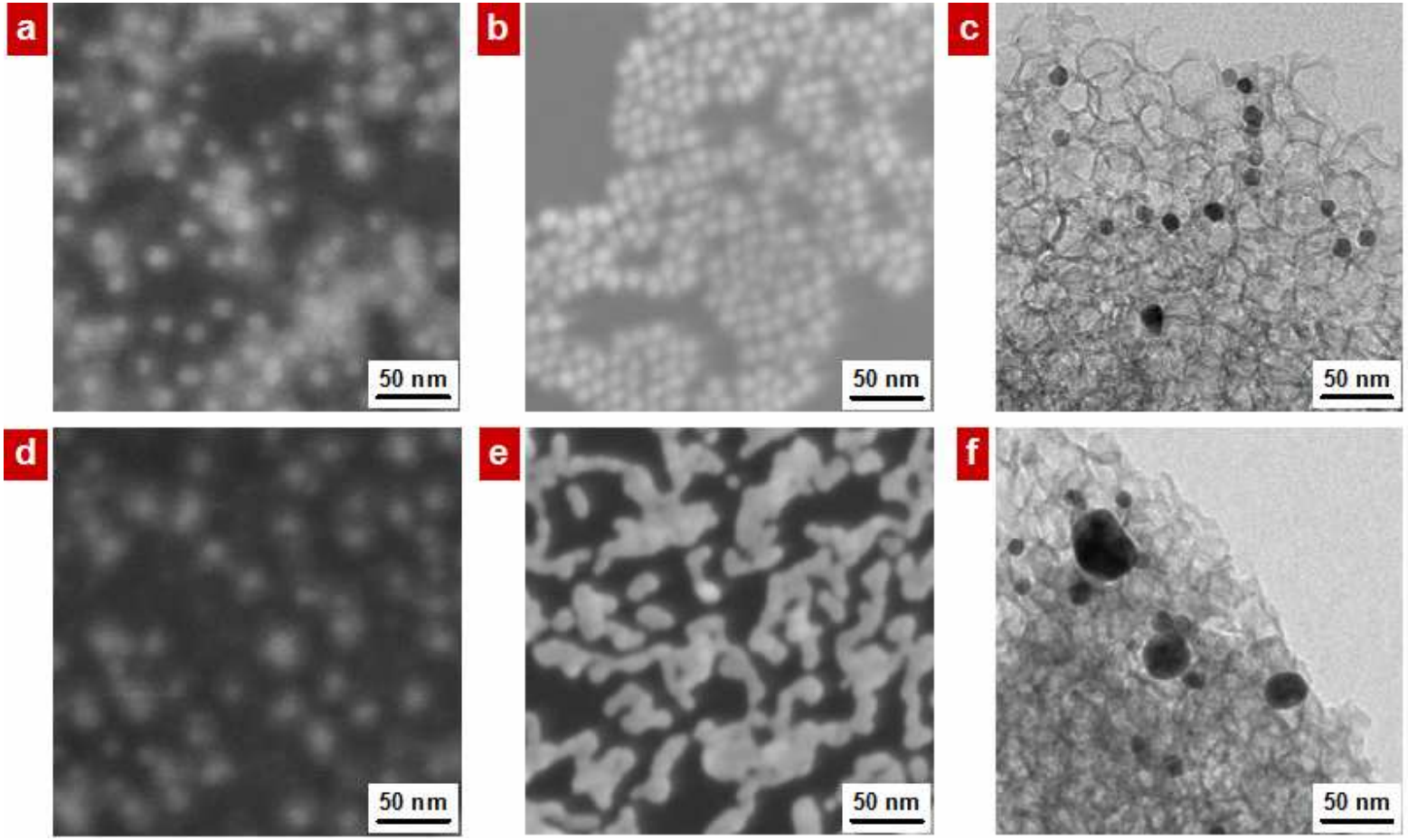

Figure 6